# Theoretical analysis of warping operators for non-ideal shallow water waveguides

Haiqiang Niu,[a] Renhe Zhang, and Zhenglin Li
*State Key Laboratory of Acoustics, Institute of Acoustics, Chinese Academy of Sciences, Beijing 100190, People's Republic of China*

(Received 28 October 2013; revised 17 May 2014; accepted 23 May 2014)

Signals propagating in waveguides can be decomposed into normal modes that exhibit dispersive characteristics. Based on the dispersion analysis, the warping transformation can be used to improve the modal separability. Different from the warping transformation defined using an ideal waveguide model, an improved warping operator is presented in this paper based on the beam-displacement ray-mode (BDRM) theory, which can be adapted to low-frequency signals in a general shallow water waveguide. For the sake of obtaining the warping operators for the general waveguides, the dispersion formula is first derived. The approximate dispersion relation can be achieved with adequate degree of accuracy for the waveguides with depth-dependent sound speed profiles (SSPs) and acoustic bottoms. Performance and accuracy of the derived formulas for the dispersion curves are evaluated by comparing with the numerical results. The derived warping operators are applied to simulations, which show that the non-linear dispersion structures can be well compensated by the proposed warping operators. © *2014 Acoustical Society of America*.
[http://dx.doi.org/10.1121/1.4883370]

PACS number(s): 43.30.Bp, 43.30.Es, 43.60.Hj, 43.60.Pt [SED] Pages: 53–65

## I. INTRODUCTION

In underwater acoustics, the normal mode theory is an effective method to describe and analyze the acoustic field. According to the normal mode theory,[1,2] signals propagating in a shallow water waveguide can be decomposed into a set of modal components, which exhibit dispersive characteristics. There are various studies based on the dispersive effect of normal modes such as the analysis of dispersive characteristics,[3–6] source localization,[7] dispersion removal,[8,9] and geoacoustic inversion.[10–17] In most studies, the modal characteristics are extracted from the time-frequency representations (TFRs) to analyze the signals in the time-frequency domain.[18–20] In the time-frequency domain, each mode is described by the dispersion curve, which can be used as an input for many applications. However, for some ocean environments, modes are not always distinguishable with the conventional TFR methods. Recently, warping operators have been introduced as signal-processing tools to improve the modal separability.[21–27] The warping transforms are designed to compensate for the dispersive effect and isolate the modal components. Thus the warping transformation facilitates the extraction of modal features.

The form of warping transformation is related to the dispersion of waveguides. The warping operators used in Refs. 21–24 were built based on an ideal waveguide with perfect reflection boundaries. The Pekeris unitary operator introduced by Touzé *et al.*[25] was built using an approximate dispersion formula for a Pekeris model and based on this operator, frequency and time-frequency representations were developed to filter modal components. In Ref. 25, the dispersion relation for the Pekeris model was derived based on the approximation $v^p v^g = c_1^2$, where $v^p$ and $v^g$ are phase velocity and group velocity of acoustic waves and $c_1$ is the sound speed of sea water. Although this approximation holds for the ideal waveguide, it has no theoretical base for the Pekeris waveguide as stated in Ref. 25. Without using that approximation, a more accurate dispersion formula for the Pekeris waveguide was presented in Ref. 27 using the BDRM theory,[28,29] which provides the concise group velocity and modal attenuation formulas by using the reflection coefficients and cycle distance of eigen-ray. Theoretically, different waveguide models (e.g., ideal waveguide models or Pekeris models) lead to different forms of warping operators, although the warping operators derived from the ideal waveguide may be probably adapted to many low-frequency shallow-water scenarios.[21,22] This leads to a question: In theory, what is the form of the warping operator for the general waveguides with arbitrary sound speed profiles of sea water and fluid bottoms?

The key to the derivation of warping operators is to obtain the dispersion relation (frequency $f$ as a function of time $t$). As an extension of Ref. 27, the dispersion relation for the Pekeris case is discussed in more detail in this paper. The whole frequency band is divided into two intervals bounded by the Airy frequency for which both the dispersion formulas are given. Further, the derivation of the warping transformation for the general waveguide with a non-isovelocity sound speed profile, which usually exists in mid-latitude shallow water, is given by taking advantage of the BDRM theory. Although it is difficult to obtain the exact dispersion formula in a general waveguide, we can get an approximate dispersion formula with adequate precision by including the first-order terms of Taylor expansion. Then the warping operators can be derived by integrating the

[a]Author to whom correspondence should be addressed. Electronic mail: nhq@mail.ioa.ac.cn

dispersion formula. The performance of the proposed warping operator is verified for different waveguide models, and the comparison of different warping operators is given when there is an environmental mismatch in the warping model.

It should be stressed that the derived warping operators in this paper are only adapted to the low-frequency shallow-water waveguides in theory, i.e., the surface-reflected bottom-reflected (SR-BR) modes. This will be discussed in detail in the following sections. In addition, the bottom is assumed to be a fluid medium where the shear waves are neglected.

The paper is organized as follows. Section II briefly describes the BDRM theory. In Sec. III, the derivation of the dispersion relation in shallow water is given. In this section, the dispersion relation of Pekeris model derived from the BDRM theory is first reviewed, followed by the case of an inhomogeneous waveguide with a depth-varying sound speed profile in sea water. Section IV presents the warping operators for the general waveguide based on the dispersion formula derived in Sec. III. Simulations are performed to validate the proposed warping transformation. Finally, Sec. V provides the summary.

## II. BRIEF DESCRIPTION OF BDRM THEORY

The BDRM theory[28] is one of the normal mode methods. The received pressure field, excited by a harmonic point source after propagation in the waveguide, can be expressed as a sum of WKBZ modes,[28,30] the horizontal wavenumbers of which satisfy the eigen-equation

$$2\int_{\zeta_{l1}}^{\zeta_{l2}}\sqrt{k^2(z)-\mu_l^2}\,dz+\varphi_1(\mu_l)+\varphi_2(\mu_l)=2l\pi,\quad l=0,\,1,\,2,\ldots, \tag{1}$$

and

$$\beta_l=\frac{-\ln|V_1(\mu_l)V_2(\mu_l)|}{S(\mu_l)+\delta_1(\mu_l)+\delta_2(\mu_l)}, \tag{2}$$

where

$$S(\mu_l)=2\int_{\zeta_{l1}}^{\zeta_{l2}}\frac{\mu_l\,dz}{\sqrt{k^2(z)-\mu_l^2}}, \tag{3}$$

$$\delta_1(\mu_l)=-\frac{\partial\varphi_1(\mu_l)}{\partial\mu_l}\bigg|_{\omega}, \tag{4}$$

$$\delta_2(\mu_l)=-\frac{\partial\varphi_2(\mu_l)}{\partial\mu_l}\bigg|_{\omega}. \tag{5}$$

In Eqs. (1) and (2), $\mu_l$ is the horizontal wavenumber, $\beta_l$ is the modal attenuation, $\zeta_{l1}$ and $\zeta_{l2}$ are the upper and lower turning or reflecting depths, respectively, and $k(z)$ is the wavenumber in sea water. $V_1(\mu_l)$ and $V_2(\mu_l)$ are the plane wave reflection coefficients on the upper boundary at depth $\zeta_{l1}$ and the lower boundary at depth $\zeta_{l2}$. $\varphi_1$ and $\varphi_2$ are the phases of $V_1$ and $V_2$, respectively. $S(\mu_l)$ in Eq. (3) is the cycle distance of eigen-ray in sea water. $\delta_1(\mu_l)$ in Eq. (4) and $\delta_2(\mu_l)$ in Eq. (5) are the beam displacements of the eigen-ray on the upper and lower boundaries, which represent the corrections for the ray length, i.e., $S(\mu_l)+\delta_1(\mu_l)+\delta_2(\mu_l)$ constitutes the ray length over one period.

As an example, Fig. 1 illustrates the eigen-ray expressed by the BDRM theory in the shallow-water waveguide.

The modal group velocity can be expressed as[28]

$$v_l^g=\frac{S(\mu_l)+\delta_1(\mu_l)+\delta_2(\mu_l)}{T(\mu_l)+\tau_1(\mu_l)+\tau_2(\mu_l)}, \tag{6}$$

where

$$T(\mu_l)=2\int_{\zeta_{l1}}^{\zeta_{l2}}\frac{k(z)dz}{c(z)\sqrt{k^2(z)-\mu_l^2}}, \tag{7}$$

$$\tau_1(\mu_l)=\frac{\partial\varphi_1(\mu_l)}{\partial\omega}\bigg|_{\mu_l}, \tag{8}$$

$$\tau_2(\mu_l)=\frac{\partial\varphi_2(\mu_l)}{\partial\omega}\bigg|_{\mu_l}. \tag{9}$$

$\tau_1(\mu_l)$ and $\tau_2(\mu_l)$ are the time delays corresponding to the beam displacements $\delta_1(\mu_l)$ and $\delta_2(\mu_l)$ at the upper and lower boundaries. $c(z)$ is the sound speed in sea water.

## III. DISPERSION RELATION IN SHALLOW WATER

The dispersion relation is derived from the BDRM theory. The analytic expressions of instantaneous frequency (i.e., time-frequency dispersion curves) are obtained by combining the eigen-equation [i.e., Eq. (1)] and the expression of modal group velocity [i.e., Eq. (6)].

### A. Dispersion relation for Pekeris waveguide

First, we focus on the case of a Pekeris waveguide. Actually, an approximate formulation of the dispersion relation for the Pekeris model was given as Eq. (3) in Ref. 25. However, as mentioned in Sec. I, this formulation is based on the approximation $v^p v^g = c_1^2$. Different from that, a more accurate dispersion formula derived from BDRM theory was discussed in Ref. 27 for a Pekeris waveguide. For the Pekeris waveguide, the group velocity of each mode has a minimum at a certain frequency, which corresponds to the Airy phase.[1] In this scenario, the instantaneous frequency $f$

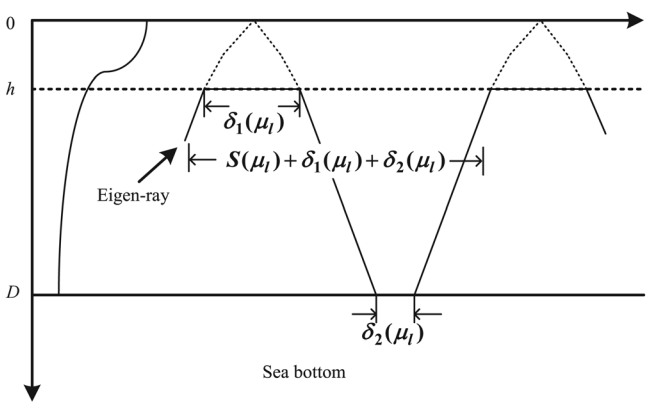


FIG. 1. Sketch illustrating eigen-ray in the shallow-water waveguide.

is a multi-valued function of time $t$. Hence to obtain the solutions, the whole frequency band is divided into two intervals bounded by the Airy frequency (i.e., the frequency corresponding to the Airy phase). Denote the cutoff frequency and the Airy frequency by $f_{cut}$ and $f_{Airy}$, respectively. Then the frequency intervals can be represented by $[f_{cut}, f_{Airy}]$ and $[f_{Airy}, +\infty]$. Actually the dispersion formula in Ref. 27 is adapted to the frequency interval $[f_{Airy}, +\infty]$. In the following, dispersion equations are discussed for these two frequency intervals, respectively.

#### 1. Dispersion relation for frequency $f > f_{Airy}$

Because the total energy of the received signal is dominated by the components over the frequency interval $[f_{Airy}, +\infty]$, this part of the group velocity curve is more important at long ranges. For a more detailed derivation of the dispersion formula for this frequency band, the readers can be referred to Ref. 27. Here we just briefly give the main steps on the derivation.

For a homogeneous water column, the cycle distance in Eq. (3) and the travel time of eigen-ray in Eq. (7) become

$$S(\mu_l) = 2D\frac{\mu_l}{\sqrt{k_1^2 - \mu_l^2}} \tag{10}$$

and

$$T(\mu_l) = 2D\frac{k_1}{c_1\sqrt{k_1^2 - \mu_l^2}}, \tag{11}$$

where $k_1$ and $c_1$ denote the wavenumber and the sound speed of sea water, respectively. $D$ is the water depth. In this case, the beam displacement $\delta_1(\mu_l)$ and the time delay $\tau_1(\mu_l)$ at the sea surface vanish. For frequency $f > f_{Airy}$, we have the approximate relations $\delta_2(\mu_l) \ll S(\mu_l)$ and $\tau_2(\mu_l) \ll T(\mu_l)$. Thus the modal group velocity becomes

$$\begin{aligned} v_l^g &= \frac{S(\mu_l) + \delta_2(\mu_l)}{T(\mu_l) + \tau_2(\mu_l)} \\ &\approx \frac{S(\mu_l)}{T(\mu_l)}\left[1 - \frac{\tau_2(\mu_l)}{T(\mu_l)} + \frac{\delta_2(\mu_l)}{S(\mu_l)} - \frac{\tau_2(\mu_l)}{T(\mu_l)}\frac{\delta_2(\mu_l)}{S(\mu_l)} + \frac{\tau_2^2(\mu_l)}{T^2(\mu_l)}\right]. \end{aligned} \tag{12}$$

Neglect the high-order terms in Eq. (12), and the modal group velocity can be approximated by

$$v_l^g \approx \frac{S(\mu_l)}{T(\mu_l)}(1+\epsilon), \tag{13}$$

where

$$\epsilon = \frac{\delta_2(\mu_l)}{S(\mu_l)} - \frac{\tau_2(\mu_l)}{T(\mu_l)}. \tag{14}$$

Inserting Eqs. (10) and (11) into Eq. (13) yields

$$v_l^g = \frac{\mu_l c_1}{k_1}(1+\epsilon). \tag{15}$$

On the other hand, the modal group velocity can also be written as

$$v_l^g = \frac{R}{t}, \tag{16}$$

where $R$ is the distance between the source and the hydrophone, and $t$ is the travel time of the wave-packet, satisfying $t \geq R/c_1$. By combining Eqs. (15) and (16), the horizontal wavenumber can be written in terms of time $t$,

$$\mu_l = \frac{k_1 R}{c_1 t(1+\epsilon)}. \tag{17}$$

For the Pekeris waveguide, Eq. (1) can be written as

$$2D\sqrt{k_1^2 - \mu_l^2} - \pi + \varphi_b = 2(l-1)\pi, \quad l = 1, 2, \ldots, \tag{18}$$

where $\varphi_b$ is the phase of the bottom reflection coefficient. By inserting Eq. (17) into Eq. (18) and replacing $k_1$ with $2\pi f/c_1$, the instantaneous frequency can be obtained,

$$f(t') = \frac{\left(2l - 1 + \frac{2\phi_b(t')}{\pi}\right)c_1 t'}{4D\sqrt{t'^2 - \left(\frac{R}{c_1}\right)^2}}, \tag{19}$$

where $t' = t(1+\epsilon)$ and $\varphi_b(t) = -2\phi_b(t)$. Because the horizontal wavenumber can be expressed as a function of time $t$, the phase $\varphi_b$ or $\phi_b$ can be also written in the time-dependent form, which will be discussed in Sec. IV B. For further simplification, Eq. (19) can be expanded as a function of $t'$ into a Taylor series around $t$,

$$f(t) = \hat{f}(t) + \hat{f}'(t)\cdot t\epsilon, \tag{20}$$

where

$$\hat{f}(t) = \frac{\left(2l - 1 + \frac{2\phi_b(t)}{\pi}\right)c_1 t}{4D\sqrt{t^2 - \left(\frac{R}{c_1}\right)^2}}. \tag{21}$$

In Eq. (20), $\hat{f}'(t)$ denotes the derivative of $\hat{f}(t)$ with respect to the argument $t$. Note that the first term $\hat{f}(t)$ on the right hand side of Eq. (20) is exactly the result obtained in Ref. 25. Actually the effect of beam displacement, which is the second term on the right hand side of Eq. (20), was not considered in Ref. 25. To simplify Eq. (20), $\hat{f}'(t)$ and $\epsilon$ should be represented as functions of time $t$.

Denoting $\sqrt{t^2 - (R/c_1)^2}$ by $\xi(t)$ to simplify the notation, we can obtain $\hat{f}'(t)$ as a function of time $t$,

$$\hat{f}'(t) = \frac{c_1}{4D}\left[-\frac{2l - 1 + \frac{2\phi_b}{\pi}}{\xi^3}\frac{R^2}{c_1^2} + \frac{\frac{2}{\pi}\phi_b' t}{\xi}\right], \tag{22}$$

where the prime denotes the derivative with respect to $t$.

Then the expression of $\epsilon$ is derived as follows. From Eq. (17), the horizontal wavenumber can be approximated by

$$\mu_l \approx \frac{k_1 R}{c_1 t} = \frac{\omega R}{c_1^2 t}. \tag{23}$$

With Eqs. (5), (9), and (23), the beam displacement and the time delay reduce to

$$\delta_2(\mu_l) = -\frac{2\phi_b' t}{\mu_l}, \tag{24}$$

$$\tau_2(\mu_l) = -\frac{2\phi_b' R}{\mu_l c_1^2}. \tag{25}$$

Inserting Eqs. (10), (11), (23), (24), and (25) into Eq. (14) yields

$$\epsilon = -\frac{\phi_b' \xi^3}{k_1 D}\frac{c_1^2}{R^2}. \tag{26}$$

Combined with Eqs. (22) and (26), the second term of Eq. (20) becomes

$$\hat{f}'(t)t\epsilon = \frac{c_1}{4D}\left[\frac{2}{\pi}\xi\phi_b' - \frac{2}{\pi}\frac{(\phi_b')^2\xi^2}{k_1 D}\frac{c_1^2 t^2}{R^2}\right]. \tag{27}$$

Note that the second term on the right hand side of Eq. (27) is generally a small quantity compared to the first term. So we neglect the second term in Eq. (27) and write the final result as

$$f(t) = \frac{\left(2l - 1 + \frac{2\phi_b(t)}{\pi}\right)c_1 t}{4D\sqrt{t^2 - \left(\frac{R}{c_1}\right)^2}} + \frac{c_1}{4D}\frac{2}{\pi}\sqrt{t^2 - \left(\frac{R}{c_1}\right)^2}\,\phi_b'(t). \tag{28}$$

Equation (28) is the derived more accurate dispersion formula for the Pekeris waveguide over the frequency band $[f_{Airy}, +\infty]$ by taking account of the effect of bottom beam displacement on the modal group velocity. For comparison, the dispersion formula Eq. (3) in Ref. 25 is also rewritten as follows:

$$f^{Pek}(t) = \frac{\left(2l - 1 + \frac{2\phi_b(t)}{\pi}\right)c_1 t}{4D\sqrt{t^2 - \left(\frac{R}{c_1}\right)^2}}. \tag{29}$$

#### 2. Dispersion relation for frequency $f_{cut} < f < f_{Airy}$

Generally, the frequency interval $[f_{cut}, f_{Airy}]$ is a very narrow band for each normal mode, whereas the group velocity varies rapidly over this band. Actually modes near cutoff are weakly excited.[1] Hence the contribution of this part is insignificant at long ranges. Because this part of frequency band is of minor interest, here we just present the final form of the dispersion formula (the detailed derivation is shown in Appendix A)

$$f(t) = \sqrt{\left(\frac{(2l-1)^2}{16D^2} + \frac{1}{4\pi^2 D^2}\frac{\rho_1^2}{\rho_2^2}\frac{\left(1 - \frac{R}{c_2 t}\right)^2}{\left(\frac{c_2 R}{c_1^2 t} - 1\right)^2}\right) \Big/ \left(\frac{1}{c_1^2} - \frac{1}{c_2^2}\right)}, \tag{30}$$

where $\rho_1$, $c_1$ are the density and sound speed of water, and $\rho_2$, $c_2$ represent the density and sound speed in bottom.

Note that the dispersion relation Eq. (30) is derived in the absence of bottom absorption (see Appendix A). The derived formula Eq. (30) will be validated by the simulation in Sec. IV C 1.

### B. Dispersion relation for a non-isovelocity waveguide

Generally, the sound speed in shallow water is depth-dependent. In this part, we present the generalized warping operator adapted to the waveguide with a depth-varying SSP in sea water. Because we are mainly concerned about the long-range propagation, the dispersion relation for frequency interval $[f_{cut}, f_{Airy}]$, which is similar to that of the Pekeris waveguide, is not given in this paper. In the following derivation, the interval $[f_{Airy}, +\infty]$ will be our concerned frequency band. As mentioned in Sec. I, only the SR-BR modes are considered in the derivation, which means that the upper turning depth $\zeta_{l1} = 0$ and the lower turning depth $\zeta_{l2} = D$.

As the sound speed of sea water is depth-dependent, we represent the SSP as

$$c(z) = \bar{c}[1 - a(z)], \tag{31}$$

where $a(z)$ denotes the quantity varying with depth (commonly, $|a(z)| \ll 1$) and $\bar{c}$ is the average sound speed, which satisfies

$$\bar{c} = \frac{1}{D}\int_0^D c(z)dz. \tag{32}$$

Actually, the expression of SSP may have various forms in theory. However, the form in Eq. (31) proves convenient in the derivation of dispersion relation. Combination of Eqs. (31) and (32) yields

$$\int_0^D a(z)dz = 0. \tag{33}$$

Equation (33) is very helpful in the following derivation. The wavenumber of sea water can then be written as

$$k(z) = \frac{\omega}{c(z)} \approx \bar{k}[1 + a(z)], \tag{34}$$

where $\bar{k} = \omega/\bar{c}$.

For the case of depth-varying SSP, the integrals in Eqs. (1), (3), and (7) can be simplified by a Taylor expansion around the average sound speed. By expanding the kernel of integral into a Taylor series and retaining the first-order term, the cycle distance in Eq. (3) can be written as

$$S(\mu_l) \cong 2\int_0^D \mu_l \left[\frac{1}{\sqrt{\bar{k}^2-\mu_l^2}} - \frac{\bar{k}}{\left(\bar{k}^2-\mu_l^2\right)^{3/2}} a(z)\bar{k}\right] dz$$
$$= 2\left[\frac{D\mu_l}{\sqrt{\bar{k}^2-\mu_l^2}} - \frac{\mu_l \bar{k}^2}{\left(\bar{k}^2-\mu_l^2\right)^{3/2}} \cdot \int_0^D a(z)dz\right]. \tag{35}$$

Taking account of Eq. (33), Eq. (35) can be simplified to

$$S(\mu_l) \approx \frac{2D\mu_l}{\sqrt{\bar{k}^2-\mu_l^2}}. \tag{36}$$

According to the same approach as in the preceding text, the expression of the travel time of eigen-ray can be obtained as

$$T(\mu_l) \cong 2\int_0^D \left[\frac{\bar{k}}{\bar{c}\sqrt{\bar{k}^2-\mu_l^2}} + \frac{\bar{k}^2-2\mu_l^2}{\bar{c}\left(\bar{k}^2-\mu_l^2\right)^{3/2}} a(z)\bar{k}\right] dz$$
$$= \frac{2D\bar{k}}{\bar{c}\sqrt{\bar{k}^2-\mu_l^2}}. \tag{37}$$

Equations (36) and (37) are the results by considering the first-order approximation of the Taylor expansion. By taking advantage of Eq. (33), the expressions of the cycle distance and the corresponding travel time are concise.

Note that Eqs. (36) and (37) are of the same forms as Eqs. (10) and (11). For the waveguide with a depth-dependent profile, the average sound speed $\bar{c}$ and wavenumber $\bar{k}$ are included in Eqs. (36) and (37) instead of the constant sound speed $c_1$ and wavenumber $k_1$ in homogeneous models. With the same procedures as Eqs. (12)–(16), the horizontal wavenumber can be obtained in terms of $t$,

$$\mu_l = \frac{\bar{k}R}{\bar{c}t(1+\epsilon)}. \tag{38}$$

For the SR-BR modes, the phase of the surface reflection coefficient is $-\pi$, and the phase of the bottom reflection coefficient is $\varphi_b = -2\phi_b$. Then the eigen-equation can be written as

$$2\int_0^D \sqrt{k^2(z)-\mu_l^2}dz = (2l-1)\pi - \varphi_b, \quad l = 1, 2, \ldots. \tag{39}$$

Expanding the kernel of the integral into a Taylor series and retaining the first-order term, then Eq. (39) can be rewritten as

$$\int_0^D \left[\sqrt{\bar{k}^2-\mu_l^2} + \frac{\bar{k}^2 a(z)}{\sqrt{\bar{k}^2-\mu_l^2}}\right] dz = \frac{(2l-1)}{2}\pi - \frac{\varphi_b}{2},$$
$$l = 1, 2, \ldots. \tag{40}$$

By taking advantage of Eq. (33), Eq. (40) reduces to

$$D\sqrt{\bar{k}^2-\mu_l^2} = \frac{(2l-1)}{2}\pi - \frac{\varphi_b}{2}. \tag{41}$$

By inserting Eq. (38) into Eq. (41), we obtain the dispersion relation for the waveguides with a depth-varying profile in sea water,

$$f(t') = \frac{\left(2l-1+\frac{2\phi_b}{\pi}\right)\bar{c}t'}{4D\sqrt{t'^2-\left(\frac{R}{\bar{c}}\right)^2}}, \tag{42}$$

where $t' = t(1+\epsilon)$. Equation (42) is also the same as Eq. (19) in the form. Thus we expand Eq. (42) as a function of $t'$ into a Taylor series around $t$ and follow the same steps as Eqs. (20)–(27). Then the final dispersion formula for the waveguide with a depth-dependent SSP is

$$f(t) = \frac{\left(2l-1+\frac{2\phi_b}{\pi}\right)\bar{c}t}{4D\sqrt{t^2-\left(\frac{R}{\bar{c}}\right)^2}} + \frac{\bar{c}}{4D}\frac{2}{\pi}\sqrt{t^2-\left(\frac{R}{\bar{c}}\right)^2}\,\phi_b'(t). \tag{43}$$

Equation (43) is the generalized dispersion formula in shallow water that includes the first-order approximations of Taylor expansion. If the average sound speed $\bar{c}$ in Eq. (43) is replaced by the constant speed $c_1$ in the Pekeris case, then the form of Eq. (43) is exactly the same as that of Eq. (28). Actually, Eq. (43) is also the generalization of the warping operators in Refs. 21–24 for the ideal waveguides. The dispersion relation of the ideal waveguides can be derived from Eq. (43). For the ideal waveguide with a pressure-release surface and a rigid bottom, the phases of reflection coefficients at boundaries satisfy $\varphi_1 = -\pi$ and $\varphi_b = -2\phi_b = 0$. Then Eq. (43) reduces to

$$f_{id}(t) = \frac{(2l-1)ct}{4D\sqrt{t^2-\left(\frac{R}{c}\right)^2}}. \tag{44}$$

## IV. WARPING OPERATORS AND SIMULATIONS

### A. Warping operators

By the frequency integration method similar to that in Ref. 25, the warping operators for our concerned frequency interval $[f_{Airy}, +\infty]$ can be achieved from the derived dispersion relation, i.e., Eq. (43). To get the warping operators, the instantaneous phase of the received signal should be calculated. Because the instantaneous phase is a nonlinear function of time $t$, the warping operators should be designed to compensate for this nonlinearity. Because the instantaneous

frequency is the derivative of the instantaneous phase, the modal phase can then be obtained as

$$\psi_l(t) = 2\pi \int_{R/\bar{c}}^{t} f(u)du. \tag{45}$$

Inserting Eq. (43) into Eq. (45) yields

$$\psi_l(t) = \frac{2\pi}{4D}\left[(2l-1)\bar{c}\sqrt{t^2-\left(\frac{R}{\bar{c}}\right)^2} + \frac{2}{\pi}\left(\bar{c}\phi_b\sqrt{t^2-\left(\frac{R}{\bar{c}}\right)^2}\right)\right]. \tag{46}$$

Then Eq. (46) can be rewritten as

$$\psi_l(t) = 2\pi[f_{cl}\xi(t) + \chi(t)], \tag{47}$$

where

$$f_{cl} = \frac{(2l-1)\bar{c}}{4D}, \tag{48a}$$

$$\xi(t) = \sqrt{t^2-\left(\frac{R}{\bar{c}}\right)^2}, \tag{48b}$$

$$\chi(t) = \frac{\bar{c}\phi_b(t)\xi(t)}{2D\pi}. \tag{48c}$$

Actually, $f_{cl}$ is the "equivalent cutoff" frequency of mode $l$ for an ideal waveguide, where the sound speed is $\bar{c}$. $\chi(t)$, which is different from Eq. (12) in Ref. 25 in the form, represents the effect of bottom on the instantaneous phase of the received signal.

As mentioned in Ref. 25, to obtain the linear modal structures, the developed warping operator should be designed to compensate for the two phase terms $\xi(t)$ and $\chi(t)$. Note that in Eq. (47), $\chi(t)$ is independent of the mode number $l$ explicitly. It means that all the modes have the same expression of $\chi(t)$. Thus to compensate for it, the modulation operator $\mathbf{M}_q$ is introduced as[25]

$$(\mathbf{M}_q x)(t) = x(t)e^{i2\pi q(t)}, \tag{49}$$

where $x(t)$ is the received signal and $q(t) = -\chi(t)$. For the sake of compensating for the first phase term $f_{cl}\xi(t)$ in Eq. (47), the time-warping operator $\mathbf{W}_w$ is given by[25]

$$(\mathbf{W}_w x)(t) = |w'(t)|^{1/2} x[w(t)], \tag{50}$$

where $w(t)$ is the warping function, and satisfies

$$w(t) = \xi^{-1}(t) = \sqrt{t^2 + \frac{R^2}{\bar{c}^2}}. \tag{51}$$

By combining the operators $\mathbf{W}_w$ and $\mathbf{M}_q$, the warping operator for the general shallow water waveguide can be constructed as

$$(\mathbf{O}_{w,q}x)(t) = (\mathbf{W}_w\mathbf{M}_q x)(t) = \left|\frac{t}{w(t)}\right|^{1/2} x[w(t)]e^{i2\pi q[w(t)]}. \tag{52}$$

Equations (47) and (52) are the instantaneous phase and the corresponding warping operator, respectively. For the ideal waveguide, it is easy to derive the corresponding warping operators. From Eq. (44), the instantaneous phase for an ideal waveguide can be obtained as

$$\psi_{id}(t) = 2\pi f_{cl}\sqrt{t^2 - \frac{R^2}{c^2}}, \tag{53}$$

where the corresponding cutoff frequency is

$$f_{cl} = \frac{(2l-1)c}{4D}. \tag{54}$$

Then the warping operator for ideal waveguides can be simplified to

$$(\mathbf{O}_w x)(t) = (\mathbf{W}_w x)(t) = \left|\frac{t}{w(t)}\right|^{1/2} x[w(t)]. \tag{55}$$

Equation (55) is the warping operator used in Refs. 21–24. After the warping transformation by Eq. (52) or (55), the modal phases of the received signal become linear and each mode is mapped into a pure frequency $f_{cl}$.

### B. Calculating the phase of bottom reflection coefficient

The form of the warping operator has been obtained. To implement the warping transformation, $\phi_b$ in $\chi(t)$ [i.e., Eq. (48c)] should be expressed as a function of time $t$. The phase of the bottom reflection coefficient is related to the bottom models. Different bottom models, e.g., semi-infinite homogeneous bottom or multi-layered media, lead to different expressions of $\phi_b$. In addition to the bottom models, the bottom absorption also has an effect on the phase $\phi_b$ theoretically. Here we just briefly present the final results for a homogeneous fluid bottom. For a more detailed derivation, the reader is referred to Ref. 27. The case including the bottom absorption is also rewritten in Appendix B.

Neglecting the bottom absorption, the phase of the bottom reflection coefficient can be written as

$$\varphi_b(\mu_l) = -2\arctan\left(\frac{\rho_1\sqrt{\mu_l^2 - k_2^2}}{\rho_2\sqrt{k_1^2 - \mu_l^2}}\right), \tag{56}$$

where $k_2$ represents the wavenumber of the bottom half-space, and $\rho_1$, $\rho_2$ are the densities of water and bottom, respectively. By inserting Eq. (23) into Eq. (56), $\phi_b$ can then be obtained as a function of $t$,

$$\phi_b(t) = \arctan\left(\frac{\rho_1 c_1\sqrt{\left(\frac{Rc_2}{c_1^2 t}\right)^2 - 1}}{\rho_2 c_2\sqrt{1-\left(\frac{R}{c_1 t}\right)^2}}\right). \tag{57}$$

In Eq. (57), $c_2$ is the sound speed of bottom, and the time $t$ satisfies $R/c_1 \le t \le Rc_2/c_1^2$.

If the bottom absorption is considered, the phase $\varphi_b$ of the bottom reflection coefficient can be obtained by performing a few steps of mathematical operations (see Appendix B):

$$\varphi_b(t) = -\arctan\left(\frac{2\rho_1 c_1 \rho_2 c_2 \sqrt{1-\frac{R^2}{c_1^2 t^2}}\left(\sqrt{\left[\frac{c_2^2}{c_1^2}\frac{R^2}{c_1^2 t^2}-(1-b^2)\right]^2+4b^2}\right)^{1/2}\cos\frac{\phi_1}{2}}{\rho_2^2 c_2^2\left(1-\frac{R^2}{c_1^2 t^2}\right)-\rho_1^2 c_1^2\sqrt{\left[\frac{c_2^2}{c_1^2}\frac{R^2}{c_1^2 t^2}-(1-b^2)\right]^2+4b^2}}\right), \tag{58}$$

where

$$\cos\frac{\phi_1}{2} = \sqrt{\frac{1}{2}+\frac{1}{2}\frac{\frac{c_2^2}{c_1^2}\frac{R^2}{c_1^2 t^2}-(1-b^2)}{\left[\left(\frac{c_2^2}{c_1^2}\frac{R^2}{c_1^2 t^2}-(1-b^2)\right)^2+4b^2\right]^{1/2}}}. \tag{59}$$

In Eqs. (58) and (59), argument $b$ satisfies $\alpha = bk_2$, with $\alpha$ being the absorption coefficient of bottom in nepers/meter.

### C. Simulations

In Sec. III, we have obtained the dispersion relation for waveguides with a constant SSP and a depth-varying SSP in sea water, respectively. Subsequently, the warping operators based on the dispersion formulas are derived in Sec. IV A. In this part, simulations are performed to compare the derived dispersion formulas with numerical results. Then the performance of the warping transformation is examined for different waveguide models. Further, the comparison of different warping operators is given when there is mismatch between the simulated environment and the warping model.

#### 1. Comparison of dispersion relation

The accuracy of the derived dispersion formulas is examined by comparing with the numerical results calculated by the code KRAKEN.[31] The dispersion formulas for a Pekeris model and a non-isovelocity waveguide, respectively, are investigated.

In Ref. 27, the comparison of dispersion relation is investigated for the Pekeris model including bottom absorption. Different from that, two cases of the Pekeris waveguide are considered here. In the first case, the bottom is modeled in the absence of material absorption, and then in the second case, the absorption is included. The environmental parameters of the Pekeris waveguide are shown in Fig. 2.

For the first case without the bottom absorption, Fig. 3 shows the comparison of dispersion curves calculated by different methods. As shown in Fig. 3, the dispersion curves computed by Eqs. (28) and (30), corresponding to the frequency intervals $[f_{Airy}, +\infty]$ and $[f_{cut}, f_{Airy}]$, respectively, are closer to the KRAKEN solutions compared with the results of Eq. (3) in Ref. 25. The phase $\phi_b(t)$ in Eq. (28) takes the form of Eq. (57), which is derived from the model without bottom absorption. Note that in Fig. 3, neglect of the contribution of the beam displacement causes an error of arrival time over the whole frequency band.

The second case, where the bottom absorption is included in the Pekeris model, is investigated by choosing different values of the absorption coefficient. In the simulations, the absorption coefficient $\alpha$ is taken to be $0.002k_2$ Np/m (i.e., 0.109 dB/$\lambda$, which is relatively small) and $0.02k_2$ Np/m (i.e., 1.09 dB/$\lambda$, which is relatively large), respectively. The corresponding dispersion curves are illustrated in Figs. 4 and 5. It can be seen from Figs. 4 and 5 that the results from Eqs. (28) and (58) agree well with the numerical solutions by KRAKEN for the frequency band above the Airy frequency. In addition, for comparison, Figs. 4 and 5 give the results calculated by Eqs. (28) and (57), which are still in good agreement with the numerical solutions over most frequencies. Dispersion curves computed by Eq. (3) in Ref. 25 are also shown in Figs. 4 and 5. For the scenario with significant absorption in the bottom (see Fig. 5), if the absorption is neglected in the model [i.e., the phase $\phi_b(t)$ takes the form of Eq. (57)], the errors in dispersion relation occur as the frequency approaches the cutoff. However, due to the weak energy near cutoff for long-range propagation, the effect of bottom absorption on the warping transformation is limited.

Then the dispersion formula is investigated for the waveguide in the presence of thermocline. The environment

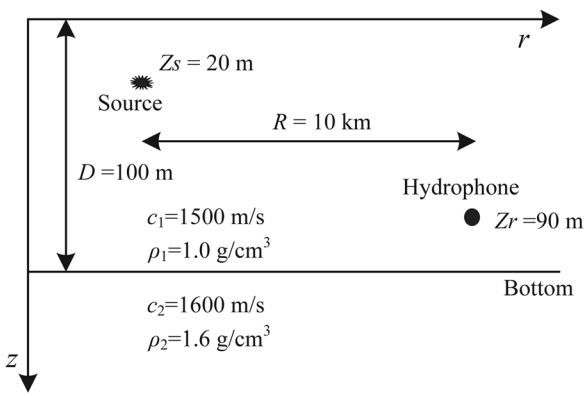


FIG. 2. Environmental parameters of the Pekeris model.

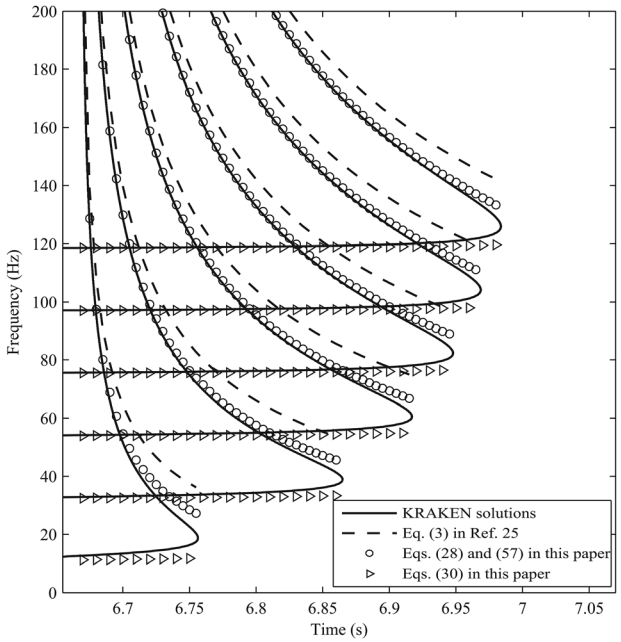


FIG. 3. Comparison of the dispersion relation calculated by different formulas in the absence of bottom absorption for Pekeris model. The curves correspond to modes 1–6, respectively.

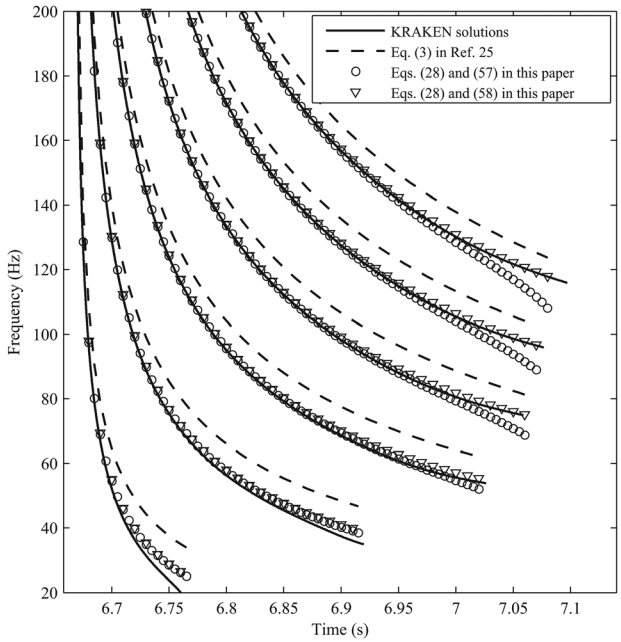


FIG. 5. Comparison of the dispersion relation calculated by different formulas in the presence of bottom absorption (absorption coefficient $\alpha = 1.09\,\mathrm{dB}/\lambda$) for Pekeris model. The curves correspond to modes 1–6, respectively.

for simulation is depicted in Fig. 6. Different from the Pekeris waveguide, the SSP of sea water, which was recorded in one of the experiments, varies in depth. The dispersion curves above the Airy frequencies are illustrated in Fig. 7. According to the environmental parameters, the numerical solutions are calculated by KRAKEN, denoted by solid lines in Fig. 7. The circles in Fig. 7 indicate the dispersion curves computed by Eqs. (43) and (58). Figure 7 shows that the modal arrival time calculated by the derived formula is very close to the numerical results for most frequencies. The relatively large error occurs in the high frequency band for the low-order normal modes (see Fig. 7). It is because the normal modes at high frequencies are not SR-BR modes in the case of a negative gradient.

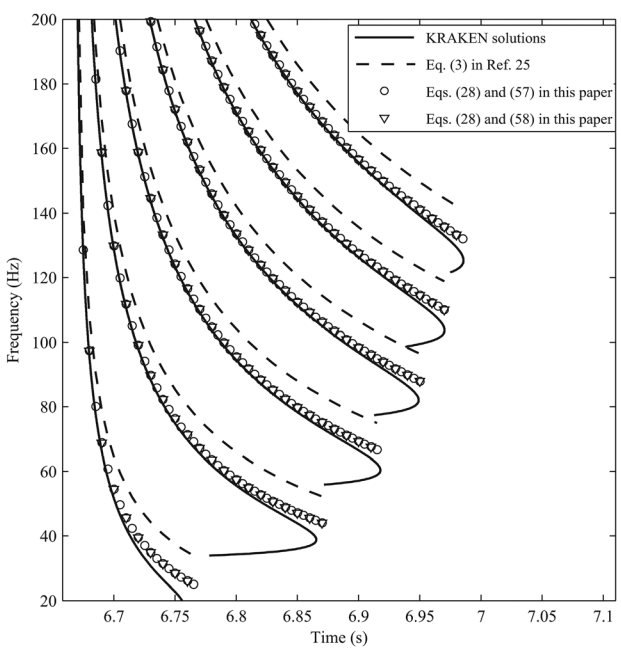


FIG. 4. Comparison of the dispersion relation calculated by different formulas in the presence of bottom absorption (absorption coefficient $\alpha = 0.109\mathrm{dB}/\lambda$) for Pekeris model. The curves correspond to modes 1–6, respectively.

### 2. Performance of warping operators

To investigate the performance of warping transformation, the derived warping operators are applied to the simulated signals propagating in waveguides. As mentioned in Sec. I, the goal of warping operators is to transform the nonlinear modes into the linear structures. To examine the validity of the derived warping operators [i.e. Eqs. (52) and (55)], simulations for different waveguides (i.e. ideal waveguide, Pekeris waveguide and non-isovelocity waveguide) are performed.

The environmental parameters in Fig. 8(a) are used to model the ideal waveguide with a pressure-release surface and a rigid bottom. Figure 8(b) shows the simulated signal received by the hydrophone at the depth of 90 m in the frequency band 20–200 Hz. The frequency spectrum of the signal after transformation [i.e., Eq. (55)] is shown in Fig.

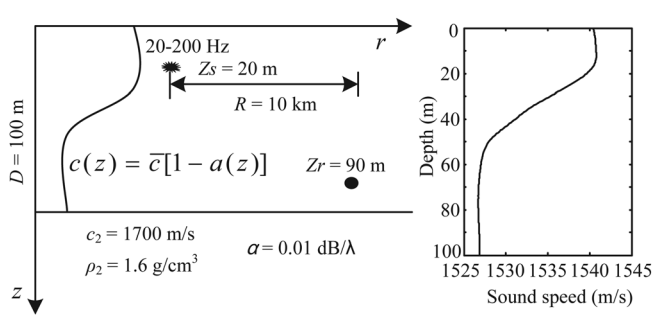


FIG. 6. Environment and geometry for the waveguide with a depth-dependent SSP.

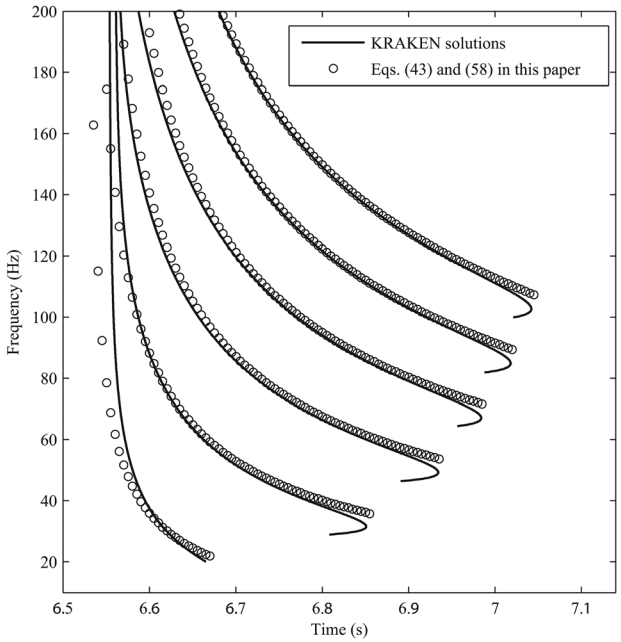


FIG. 7. Comparison of the dispersion curves between the numerical solutions and the results computed by Eqs. (43) and (58) for a non-isovelocity waveguide. The curves correspond to modes 1–6, respectively.

8(c). The dashed lines in Fig. 8(c) denote the theoretical cutoff frequencies $(2l-1)c/4D$ [i.e., Eq. (54)] for this ideal waveguide model. Figure 8(c) shows that after warping transformation, the location of each sharp peak matches well the theoretical cutoff frequency $(2l-1)c/4D$ of each mode.

For the Pekeris waveguide with a fluid bottom, the environmental parameters are shown in Fig. 9(a). Figure 9(b) exhibits the received signal in time domain with the frequency from 20 to 200 Hz. It is observed from the frequency spectrum in Fig. 9(c) that after the warping transformation, the energy of each mode is still concentrated upon the pure frequency $(2l-1)c_1/4D$, which demonstrates that the derived dispersion formula Eq. (28) and warping operator Eq. (52) are accurate for Pekeris model.

Finally, the performance of the warping operator is examined for the general waveguide with a depth-varying profile. The waveguide is modeled with a SSP measured in a summer experiment. The configuration is shown in Fig. 10(a). The frequency band of the simulated signal is 20–200 Hz, and the broadband signal in time domain is given in Fig. 10(b). Figure 10(c) shows the result of frequency spectrum from the warping operator Eq. (52), which is applied to the original received signal. By taking advantage of Eqs. (48b), (48c), and (52), the phase of the received signal is transformed into linear structures successfully and the location of each peak in frequency spectrum corresponds to the theoretical frequency, i.e., Eq. (48a).

### 3. Model mismatch performance

For experimental data, there is always mismatch between the warping model and the realistic ocean waveguide. Here we investigate the effect of model mismatch on the performance of warping transformation. Note that the warping transformation based on the ideal waveguide in Refs. 21–24 is irrelevant to the bottom parameters, while the warping operators based on non-ideal waveguides [i.e., Eq. (17) in Ref. 25 and Eq. (52) in this paper] are not the case. For the realistic environment, the sound speed of the bottom is probably the primary mismatched parameter, and here it is considered as the mismatched parameter in simulations.

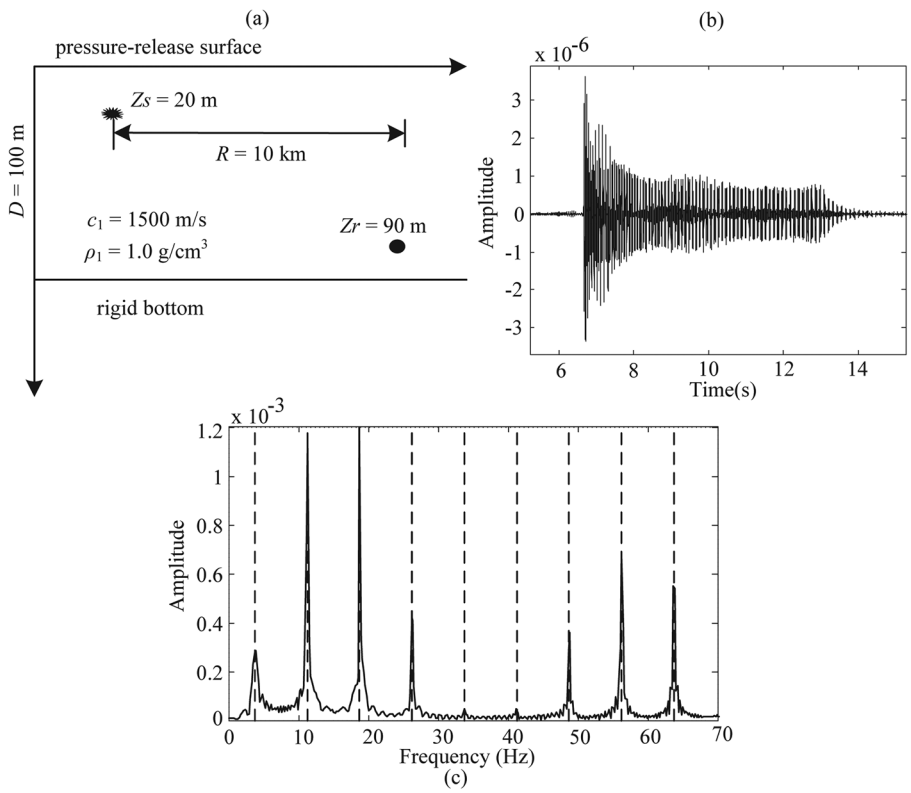


FIG. 8. Warping transformation for the ideal waveguide. (a) Environmental parameters of the ideal waveguide with a pressure-release surface and a rigid bottom. (b) Simulated signal in time domain received by the hydrophone at the depth of 90 m with frequency band 20–200 Hz. (c) Frequency spectrum of the warped signal, i.e., warping by Eq. (55). The dashed lines denote the theoretical cutoff frequencies $(2l-1)c/4D$, i.e., Eq. (54).

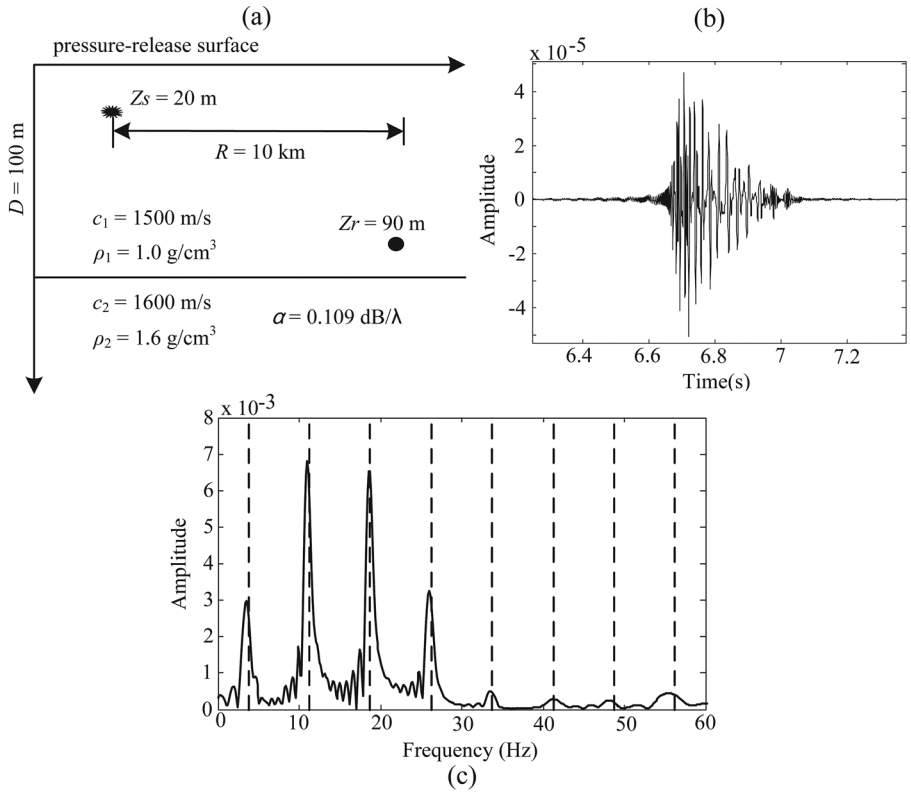


FIG. 9. Warping transformation for Pekeris waveguide. (a) Environmental parameters of the Pekeris waveguide with a pressure-release surface and a fluid bottom. (b) Simulated signal in time domain received by the hydrophone at the depth of 90 m with frequency band 20–200 Hz. (c) Frequency spectrum of the warped signal, i.e., warping by Eq. (52). The dashed lines denote the "equivalent cutoff" frequencies $(2l-1)c_1/4D$.

In the following, for simplicity, the warping based on the ideal waveguide[21–24] is called ideal-warping, the warping based on an approximate Pekeris waveguide[25] is called Pekeris-warping, and the methodology proposed in this paper is called BDRM-warping. The comparison of these three different warping results is given in the following simulations.

Examples of Pekeris waveguide are taken to illustrate the effect of bottom speed mismatch on the warping. The environmental parameters of simulated Pekeris waveguide are shown in Fig. 11, where the bottom sound speed is 1650 m/s.

First, the frequency spectra after the three different warping transformations without model mismatch are given

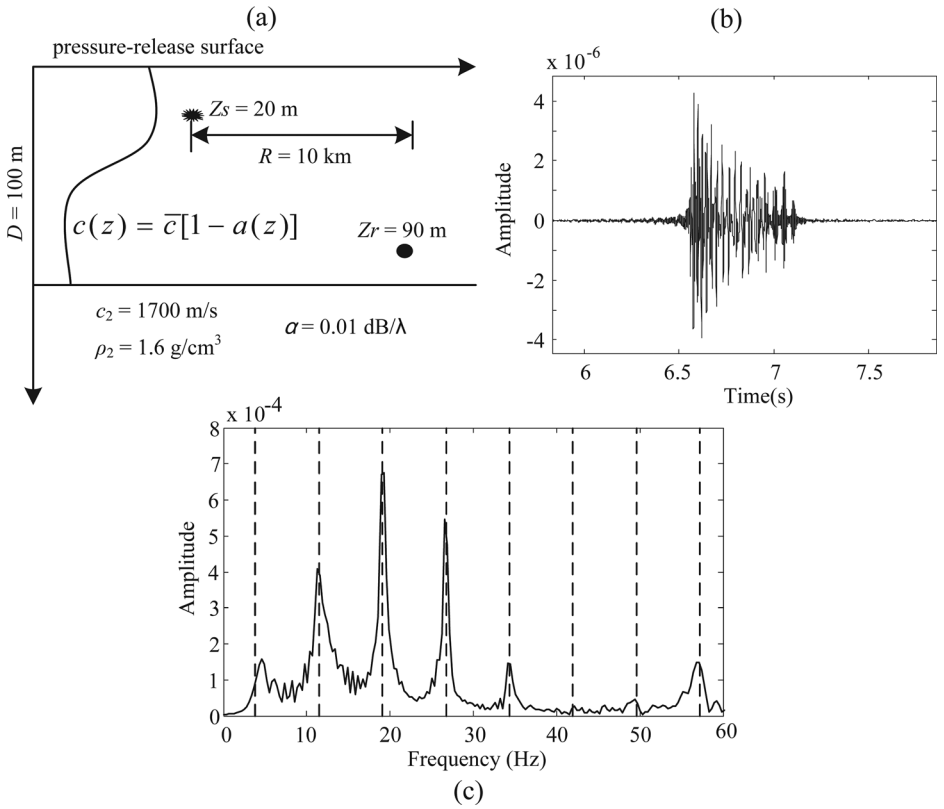


FIG. 10. Warping transformation for the general waveguide with a depth-varying profile in sea water. (a) Environmental parameters of the waveguide with a depth-varying profile in sea water and a fluid bottom. (b) Simulated signal in time domain received by the hydrophone at the depth of 90 m with frequency band 20–200 Hz. (c) Frequency spectrum of the warped signal, i.e., transformation by Eq. (52). The dashed lines denote the "equivalent cutoff" frequencies $(2l-1)\bar{c}/4D$, i.e., Eq. (48a).

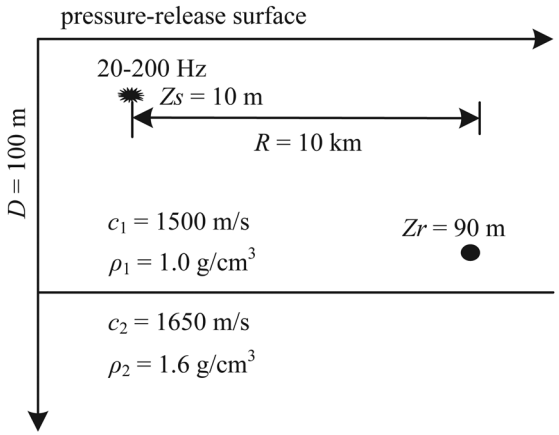


FIG. 11. Environment and geometry for the simulated Pekeris waveguide with the bottom speed 1650 m/s.

in Fig. 12(a). As shown in Fig. 12(a), compared with the results of ideal-warping and Pekeris-warping, the spectrum after BDRM-warping has sharper peaks and the locations of these peaks are much closer to the theoretical frequencies $(2l-1)c_1/4D$.

Then we consider the case where the bottom speed used in warping model mismatches the simulated environment. Now suppose that the values of bottom speed used in warping model are 1600 and 1700 m/s, respectively (i.e., the errors are −50 and 50 m/s with respect to the simulated environment). Figure 12(b) shows the frequency spectra of the received signal with bottom speed $c_2 = 1600$ m/s in warping model after ideal-, Pekeris-, and BDRM-warping, respectively. Similarly, the results are shown in Fig. 12(c) when the bottom speed is taken to be 1700 m/s in the warping transformations. It is shown from Figs. 12(b) and 12(c) that the spectra after BDRM-warping still have sharp peaks around the theoretical frequencies when there is bottom speed mismatch between warping model and the simulated environment. The simulations demonstrate that the BDRM-warping is a robust transformation with respect to the model mismatch. Another advantage of the robustness is that we can determine the mode number of the filtered mode because each of the peaks in spectrum is close to the theoretical frequency $(2l-1)c_1/4D$.

## V. SUMMARY

The warping transformation provides an effective method to separate the normal modes for impulsive signals. Different from the warping operator based on the ideal model hypothesis, this study presents an improved warping operator based on the BDRM theory, which can be adapted to low-frequency signals in general shallow water waveguides. To obtain the warping operators, the dispersion formulas for different waveguide models are derived from BDRM theory. By including the bottom beam displacement and utilizing the approximation of Taylor expansion, we obtain a more accurate dispersion relation. After the transformation with the improved warping operators, the instantaneous phase of the received signal is linear in time.

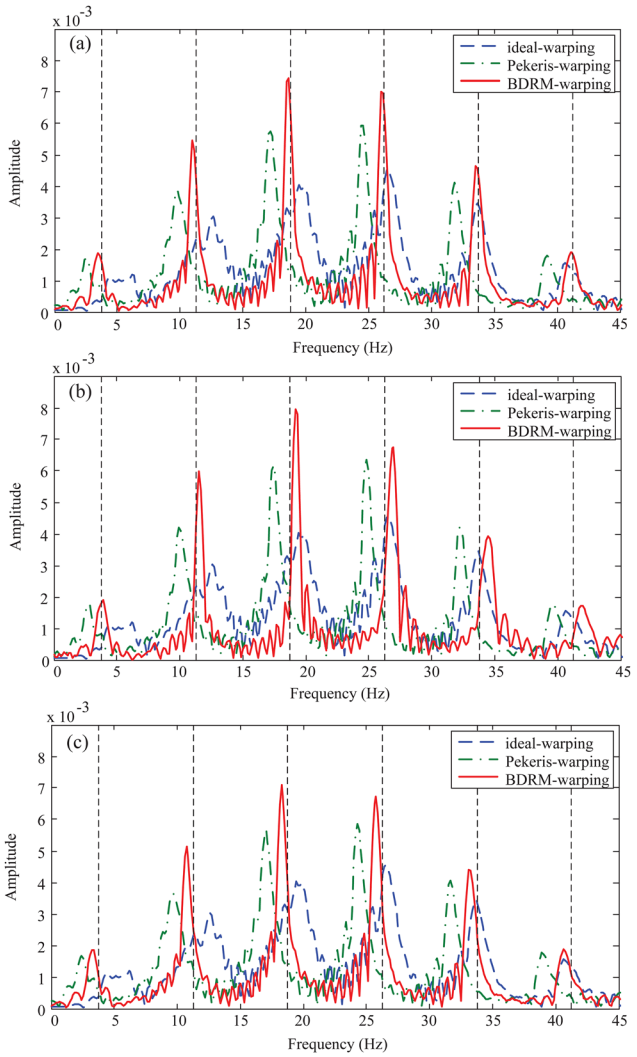


FIG. 12. (Color online) Comparison of the frequency spectra for different warping transformations. (a) Warping transformations without model mismatch (i.e., the bottom sound speed in warping model is 1650 m/s). (b) Warping transformations with model mismatch. The bottom sound speed in warping model is 1600 m/s with an error −50 m/s. (c) Warping transformations with model mismatch. The bottom sound speed in warping model is 1700 m/s with an error 50 m/s. In (a), (b), and (c), the dashed straight lines denote the theoretical frequencies $(2l-1)c_1/4D$.

The derived dispersion relation and the corresponding warping operators are validated by numerical simulations. By comparing with the numerical results, the dispersion formulas are shown to be highly accurate. The corresponding warping operators have been applied to the simulated signals successfully. Each warped mode is an approximate sinusoid corresponding to its cutoff or "equivalent cutoff" frequency. Once the original signal is transformed into warped modes, the conventional modal filtering techniques can be used to extract the separate modes.

## ACKNOWLEDGMENTS

The authors would like to thank Professor Wenyu Luo for his helpful comments and suggestions. This work was sponsored by the National Natural Science Foundation of China under Grant Nos. 11174312 and 11074269.

## APPENDIX A: DISPERSION RELATION FOR $f_{cut} < f < f_{Airy}$

For the homogeneous fluid-bottom half-space without absorption, by taking account of the horizontal wavenumber $\mu_l \to k_2$ ($k_2$ is the bottom wavenumber) near the cutoff frequency, the phase of bottom reflection coefficient can be simply approximated by

$$\varphi_b(\mu_l) = -2\arctan\left(\frac{\rho_1\sqrt{\mu_l^2-k_2^2}}{\rho_2\sqrt{k_1^2-\mu_l^2}}\right) \approx -\frac{2\rho_1\sqrt{\mu_l^2-k_2^2}}{\rho_2\sqrt{k_1^2-\mu_l^2}}. \tag{A1}$$

By inserting Eq. (A1) into Eqs. (5) and (9), the beam displacement and the corresponding time delay can be obtained as

$$\delta_2(\mu_l) = \frac{2\rho_1}{\rho_2}\cdot\left[\frac{\mu_l}{\sqrt{\mu_l^2-k_2^2}\sqrt{k_1^2-\mu_l^2}} + \frac{\mu_l\sqrt{\mu_l^2-k_2^2}}{(k_1^2-\mu_l^2)^{3/2}}\right] \approx \frac{2\rho_1}{\rho_2}\cdot\frac{\mu_l}{\sqrt{\mu_l^2-k_2^2}\sqrt{k_1^2-\mu_l^2}} \tag{A2}$$

and

$$\tau_2(\mu_l) = \frac{2\rho_1}{\rho_2}\cdot\left[\frac{k_2}{c_2\sqrt{\mu_l^2-k_2^2}\sqrt{k_1^2-\mu_l^2}} + \frac{k_1\sqrt{\mu_l^2-k_2^2}}{c_1(k_1^2-\mu_l^2)^{3/2}}\right] \approx \frac{2\rho_1}{\rho_2}\cdot\frac{k_2}{c_2\sqrt{\mu_l^2-k_2^2}\sqrt{k_1^2-\mu_l^2}}. \tag{A3}$$

For the frequency $f \in [f_{cut}, f_{Airy}]$, the relations $\delta_2(\mu_l) \ll S(\mu_l)$ and $\tau_2(\mu_l) \ll T(\mu_l)$ do not hold any more because the beam displacement increases with decreasing frequency. Thus Eq. (6) is used in the derivation in this scenario instead of Eq. (12). Inserting Eqs. (10), (11), (A2), and (A3) into Eq. (6) yields

$$v_l^g = \frac{D\mu_l + \frac{\rho_1}{\rho_2}\frac{\mu_l}{\sqrt{\mu_l^2-k_2^2}}}{D\frac{k_1}{c_1} + \frac{\rho_1}{\rho_2}\frac{k_2}{c_2\sqrt{\mu_l^2-k_2^2}}}, \tag{A4}$$

which together with Eq. (16) leads to

$$\frac{\rho_1}{\rho_2}\frac{\mu_l - \frac{k_2R}{c_2t}}{\sqrt{\mu_l^2-k_2^2}} = D\left(\frac{k_1R}{c_1t} - \mu_l\right). \tag{A5}$$

Equation (A5) can be further simplified using the approximate relation $\mu_l \approx k_2$. In Eq. (A5), by replacing $\mu_l$ by $k_2$ except for the term $\sqrt{\mu_l^2-k_2^2}$ and solving for $\mu_l$, we obtain

$$\mu_l = \sqrt{k_2^2 + \frac{\rho_1^2}{\rho_2^2D^2}\left(\frac{k_2 - \frac{k_2R}{c_2t}}{\frac{k_1R}{c_1t} - k_2}\right)^2}. \tag{A6}$$

Similar to the procedure in Sec. III A 1, inserting Eq. (A6) into Eq. (18), and taking advantage of the relations $k_1 = 2\pi f/c_1$, $k_2 = 2\pi f/c_2$, and $\varphi_b \approx 0$, the final instantaneous frequency can be obtained as

$$f(t) = \sqrt{\left(\frac{(2l-1)^2}{16D^2} + \frac{1}{4\pi^2D^2}\frac{\rho_1^2}{\rho_2^2}\frac{\left(1-\frac{R}{c_2t}\right)^2}{\left(\frac{c_2R}{c_1^2t}-1\right)^2}\right)\Big/\left(\frac{1}{c_1^2}-\frac{1}{c_2^2}\right)}. \tag{A7}$$

## APPENDIX B: THE PHASE OF BOTTOM REFLECTION COEFFICIENT WITH BOTTOM ABSORPTION

The material absorption can be included by adding an imaginary part to the sound speed so that $c_2 = c_r - ic_i$.[1,31] Then the complex wavenumber of the bottom can be written as

$$K_2 = \frac{\omega}{c_2} = \frac{\omega}{c_r - ic_i} = \omega\frac{c_r + ic_i}{c_r^2 + c_i^2}. \tag{B1}$$

Because generally $c_i \ll c_r$, Eq. (B1) can be simplified to

$$K_2 = \frac{\omega}{c_r} + i\frac{\omega c_i}{c_r^2} = k_2 + i\alpha = k_2(1+ib), \tag{B2}$$

where $\alpha = bk_2 = \omega c_i/c_r^2$ denotes the absorption coefficient of bottom in nepers/meter. Then the reflection coefficient of bottom can be written as[1]

$$V = \frac{\rho_2\sqrt{k_1^2-\mu_l^2} - i\rho_1\sqrt{\mu_l^2-k_2^2(1+ib)^2}}{\rho_2\sqrt{k_1^2-\mu_l^2} + i\rho_1\sqrt{\mu_l^2-k_2^2(1+ib)^2}} = \frac{\rho_2\sqrt{k_1^2-\mu_l^2} - i\rho_1\sqrt{Ae^{i\phi_1}}}{\rho_2\sqrt{k_1^2-\mu_l^2} + i\rho_1\sqrt{Ae^{i\phi_1}}}, \tag{B3}$$

where $A = \sqrt{(\mu_l^2 - k_2^2(1-b^2))^2 + 4b^2k_2^4}$ and $\phi_1 = -\arctan\left[2bk_2^2/(\mu_l^2 - k_2^2(1-b^2))\right]$. Denote $M = \rho_2\sqrt{k_1^2-\mu_l^2}$, $N = \rho_1A^{1/2}\sin(\phi_1/2)$, and $P = \rho_1A^{1/2}\cos(\phi_1/2)$. Then Eq. (B3) can be reduced to

$$V = \frac{M^2 - N^2 - P^2 - i2MP}{(M-N)^2 + P^2}. \tag{B4}$$

Thus the phase of the reflection coefficient of bottom can be obtained as

$$\varphi_b = -\arctan\frac{2\rho_1\rho_2A^{1/2}\sqrt{k_1^2-\mu_l^2}\cos\frac{\phi_1}{2}}{\rho_2^2(k_1^2-\mu_l^2) - \rho_1^2A}. \tag{B5}$$

Inserting Eq. (23) into Eq. (B5), we can then obtain the phase of reflection coefficient with bottom absorption as a function of time $t$, i.e., Eqs. (58) and (59).


[1]F. B. Jensen, W. A. Kuperman, M. B. Porter, and H. Schmidt, *Computational Ocean Acoustics* (AIP, New York, 1994), Chaps. 2, 5, and 8.
[2]I. Tolstoy and C. S. Clay, *Ocean Acoustics: Theory and Experiment in Underwater Sound* (AIP, New York, 1987), Chap. 3.
[3]R. H. Zhang, J. Q. Xiao, and M. Gong, "Analysis of individual modes in shallow water," Acta Acust. **3**, 238–249 (1984).
[4]K. E. Wage, A. B. Baggeroer, and J. C. Preisig, "Modal analysis of broadband acoustic receptions at 3515 km range in the North Pacific using short-time Fourier techniques," J. Acoust. Soc. Am. **113**, 801–817 (2003).
[5]K. E. Wage, M. A. Dzieciuch, P. F. Worcester, B. M. Howe, and J. A. Mercer, "Mode coherence at mega meter ranges in the North Pacific Ocean," J. Acoust. Soc. Am. **117**, 1565–1581 (2005).
[6]I. A. Udovydchenkov and M. G. Brown, "Modal group time spreads in weakly range-dependent deep ocean environments," J. Acoust. Soc. Am. **123**, 41–50 (2008).
[7]W. Kuperman, G. D'Spain, and K. Heaney, "Long range source localization from single hydrophone spectrograms," J. Acoust. Soc. Am. **109**, 1935–1943 (2001).
[8]P. D. Wilcox, M. J. S. Lowe, and P. Cawley, "A signal processing technique to remove the effect of dispersion from guided wave signals," in *Review of Progress in Quantitative Nondestructive Valuation*, edited by D. Thompson and D. E. Chimenti (AIP Conference Proceedings, New York, 2001), pp. 555–562.
[9]D. Z. Gao, N. Wang, and H. Z. Wang, "A dedispersion transform for sound propagation in shallow water waveguide," J. Comput. Acoust. **18**, 245–257 (2010).
[10]J. X. Zhou, X. Z. Zhang, and P. H. Rogers, "Geoacoustic parameters in a stratified sea bottom from shallow water acoustic propagation," J. Acoust. Soc. Am. **82**, 2068–2074 (1987).
[11]G. Potty, J. Miller, J. Lynch, and K. Smith, "Tomographic inversion for sediment parameters in shallow water," J. Acoust. Soc. Am. **108**, 973–986 (2000).
[12]Z. L. Li, J. Yan, F. H. Li, and L. H. Guo, "Inversion for the sea bottom acoustic parameters by using the group time delays and amplitude of normal mode," Acta. Acust. **27**, 487–491 (2002).
[13]G. Potty and J. Miller, "Inversion for sediment geoacoustic properties at the New England Bright," J. Acoust. Soc. Am. **114**, 1874–1887 (2003).
[14]D. M. Zhang, Z. L. Li, and R. H. Zhang, "Inversion for the bottom geoacoustic parameters based on adaptive time–frequency analysis," Acta Acust. **30**, 415–419 (2005).
[15]Z. L. Li and R. H. Zhang, "Geoacoustic inversion based on dispersion characteristic of normal modes in shallow water," Chin. Phys. Lett. **24**, 471–474 (2007).
[16]G. Potty, J. Miller, P. Wilson, J. Lynch, and A. Newhall, "Geoacoustic inversion using combustive sound source signals," J. Acoust. Soc. Am. **124**, EL146–EL150 (2008).
[17]X. L. Zhang, Z. L. Li, and X. D. Huang, "A hybrid scheme for geoacoustic inversion," Acta Acust. **34**, 54–59 (2009).
[18]J. Hong, K. Sun, and Y. Kim, "Dispersion-based short-time Fourier transform applied to dispersive wave analysis," J. Acoust. Soc. Am. **117**, 2949–2960 (2005).
[19]C. Gervaise, S. Vallez, Y. Stephan, and Y. Simard, "Robust 2D localization of low-frequency calls in shallow waters using modal propagation modeling," Can. Acoust. **36**, 153–159 (2008).
[20]C. Ioana, A. Jarrot, C. Gervaise, Y. Stéphan, and A. Quinquis, "Localization in underwater dispersive channels using the time-frequency-phase continuity of signals," IEEE Trans. Signal Process. **58**, 4093–4107 (2010).
[21]J. Bonnel, B. Nicolas, J. Mars, and S. Walker, "Estimation of modal group velocities with a single receiver for geoacoustic inversion in shallow water," J. Acoust. Soc. Am. **128**, 719–727 (2010).
[22]J. Bonnel and N. Chapman, "Geoacoustic inversion in a dispersive waveguide using warping operators," J. Acoust. Soc. Am. **130**, EL101–EL107 (2011).
[23]J. Bonnel, C. Gervaise, B. Nicolas, and J. I. Mars, "Single-receiver geoacoustic inversion using modal reversal," J. Acoust. Soc. Am. **131**, 119–128 (2012).
[24]H. Q. Niu, R. H. Zhang, Z. L. Li, Y. G. Guo, and L. He, "Bubble pulse cancelation in the time-frequency domain using warping operators," Chin. Phys. Lett. **30**, 084301 (2013).
[25]G. Le Touzé, B. Nicolas, J. Mars, and J. Lacoume, "Matched representations and filters for guided waves," IEEE Trans. Signal Process. **57**, 1783–1795 (2009).
[26]R. Baraniuk and D. Jones, "Unitary equivalence: A new twist on signal processing," IEEE Trans. Signal Process. **43**, 2269–2282 (1995).
[27]H. Q. Niu, R. H. Zhang, and Z. L. Li, "A modified warping operator based on BDRM theory in homogeneous shallow water," Sci. China Phys. Mech. Astron. **57**, 424–432 (2014).
[28]R. H. Zhang and F. H. Li, "Beam-displacement ray-mode theory of sound propagation in shallow water (in Chinese)," Sci. China Ser. A **29**, 241–251 (1999).
[29]R. H. Zhang and Z. Lu, "Attenuation and group velocity of normal mode in shallow water," J. Sound Vib. **128**, 121–130 (1989).
[30]R. H. Zhang, Y. He, and H. Liu, "Applications of the WKBZ adiabatic mode approach to sound propagation in the Philippine Sea," J. Sound Vib. **184**, 439–451 (1995).
[31]M. B. Porter, The KRAKEN Normal Mode Program, http://oalib.hlsresearch.com/Modes/AcousticsToolbox/manualtml/kraken.html (Last viewed 11/1/2009).